Structural determination of two-dimensional YSi_2 epitaxially grown on Si(111)

C. Rogero,[1] C. Polop,[1,*] L. Magaud,[2] J. L. Sacedón,[1] P. L. de Andrés,[1] and J. A. Martín-Gago[1]
[1]*Instituto Ciencia de Materiales de Madrid–CSIC, 28049-Cantoblanco, Spain*
[2]*Laboratoire d'Etudes des Propriétés Electroniques des Solides, B.P. 166, 38042 Grenoble Cedex 9, France*
(Received 12 April 2002; published 30 December 2002)

We have used a combination of dynamical low-energy-electron diffraction and density functional formalism calculations to find a structural model for two-dimensional (2D) YSi_2 layers epitaxially grown on Si(111). Both techniques show that the geometric structure of the yttrium silicide is quite similar to other 2D rare-earth silicides. The surface termination consists of a relaxed Si-bilayer and underlying Y atoms on T_4 sites [with respect to the Si(111) interface]. The low-energy electron diffraction study shows several occurrences of minima in the *R* factor. The analysis of diffracted beams measured at non-normal incidence allows us to discriminate the spurious minima.

DOI: 10.1103/PhysRevB.66.235421 PACS number(s): 81.15.Np

I. INTRODUCTION

The understanding of the exceptional electronic properties of reduced dimensionality systems has stimulated the study of the atomic structure of ultrathin heteroepitaxial overlayers. Surface-sensitive techniques and theoretical methods have been developed during the past 30 years to describe the atomic positions of these systems with a precision of the hundredth of an angstrom. On the other hand, rare-earth (RE) silicides epitaxially grown on *n*-type Si(111) present unusually low values of the Schottky barrier height[1,2] making these films valuable for electronic devices (e.g., infrared detectors). These metallic silicides present a hexagonal structure derived from the AlB_2-type structure, resulting on graphitelike Si planes intercalated by rare-earth planes. In bulk, the Si planes contain an ordered network of vacancies, forming a $(\sqrt{3}\times\sqrt{3})R30°$ superstructure, and leading to the RE $Si_{1.7}$ stoichiometry.[3–6]

For rare-earth coverages of around 1 monolayer (ML), these silicides present a two-dimensional (2D) metallic structure, exhibiting a $p(1\times1)$ periodicity. The 2D phase for rare-earth silicides was first reported for $ErSi_2$.[3,4] From Auger-electron diffraction these authors have deduced a surface atomic geometry consisting of a bulklike Si(111) plane, 180° rotated around the surface normal with respect to the Si(111) substrate. Er atoms are located about 2.7 Å below the surface plane on T_4 sites [with respect to the Si(111) interface].[5] This model, originally proposed for $ErSi_2$, has been recently generalized for other RE Si_2. Medium-energy ion scattering (MEIS) and low-energy electron diffraction (LEED) studies have shown that the 2D $HoSi_2$ presents the same atomic arrangement.[6,7] This structural model seems to be valid even for rare-earth germanides such as $DyGe_2$.[8]

The surface region of RE Si_2 does not show Si vacancies. The formation of vacancies in the bulk of the silicide seems to be related to a release of compressive strain in the inner Si(111) planes, which are graphitelike. As a consequence, one atom out of 6 is missing, and the 1:1.7 stoichiometry is found. On the other hand, Si atoms at the surface can buckle and release strain more efficiently.[3–5]

In this paper we present a detailed determination of the atomic structure of the 2D layer of YSi_2 epitaxially grown on Si(111). The existence of the 2D phase for the YSi_2 was reported by our group.[9] In that work, we described the morphology and the main defects found on the surface. We also have proved that the surface atomic arrangement imaged by scanning tunneling microscopy is compatible with the structural model described above for Er silicides and proposed for other rare-earth silicides.

It is generally accepted that although yttrium does not have $4f$ electrons, it chemically behaves as other rare earths. Particularly, it presents the same structural phases as other rare-earth silicides. The objective of this work is twofold: first, to perform a complete determination of the atomic structure of this silicide, and second, to compare the results with other silicides to know whether there is any difference in the structural parameters induced by the presence of inner $4f$ electrons or some atomic size effect that could affect to the interlayer distances.

To achieve this objective we have employed a combination of experimental and theoretical methods. A dynamical LEED *I-V* analysis has been used to explore the atomic configuration of the silicide. We have searched for a global minimum of the Pendry *R* factor.[10] This standard procedure has allowed us to determine "best-fit" values for structural and nonstructural parameters. A difficulty with this method is that one needs to make sure that a given minimum in the multidimensional space searched is in fact the global one. Similar minima in the *R* factor could appear for multiples of the interlayer spacing in a LEED analysis.[11] When this occurs, the lower value is usually chosen to represent the "real" structure, although coincidence with other independent techniques, or plausibility arguments, are also often decisive to choose among them. For the YSi_2 silicide, we have found that the LEED analysis based purely on normal incidence presents at least two indistinguishable local minima. To decide whether one of them, or a combination of both, represent best the structure, we have extended our study by measuring curves where the incident electron beam is not normal to the surface. Furthermore, we have performed *ab initio* total-energy calculations based on the density-functional formalism (DFT). These two methods have allowed us to dis-

card the spurious minima and to determine the global one. Finally, it is interesting to notice that vibrational amplitude factors were found to be very important in this work; values for them are quite considerable and different for different layers, and the Pendry R factor sensitively depends on them as we shall see below.

Thus, by a combination of LEED experiments and DFT calculations we have arrived at a description of the surface atomic structure of the silicide. The final proposed geometric model is quite similar to the presented for other silicides. The outermost layer consists of a relaxed Si bilayer, located above the yttrium layer at about the same distance as in the bulk silicide, and the Y is in a T_4 position with respect to the Si(111) substrate. Their distances are compatible with that found for other silicides.

II. EXPERIMENTAL AND THEORETICAL DETAILS

Growth and characterization experiments were carried out at room temperature (RT), in an ultrahigh vacuum (UHV) system. The base pressure of the chamber was in the low 10^{-10} mbar range, raising to 2×10^{-9} mbar during the Y evaporation. This chamber is equipped with commercial LEED optics and an 8-bit CCD camera. We also have a scanning tunneling microscope that allow us to study the surface morphology and the quality of the grown films.[9]

n-type Si(111) wafers were used as substrate. They were cleaned *in situ* by standard methods (resistive heating up to 1200 °C followed by slow cooling), resulting in a sharp 7×7 LEED pattern. To form the 2D silicide, approximately 1 ML of Y was deposited at RT on the Si(111) 7×7 surface and subsequently annealed at 400 °C for 15 min. The silicide is characterized by a sharp $p(1\times1)$ LEED pattern with no traces of the $(\sqrt{3}\times\sqrt{3})R30°$ or the 7×7 superstructure. The evaporation rate was monitored with a quartz balance [1 ML corresponds to 7.8×10^{14} atoms/cm^2, the atoms of one Si(111) plane]. More details about the preparation can be found in previous works.[9]

LEED I-V curves were recorded at normal incidence as well as by varying the incidence angle with respect to the surface normal. We have measured them in an energy range from 50 to 450 eV and with an energy step of 1 eV. This surface has a threefold rotational symmetry; therefore, the equivalent diffracted beams were averaged and background subtracted together to produce five independent curves: (1,0), (0,1), (1,1), (2,0), and (0,2). For electron-beam incidences off normal we rotated the sample, maintaining a plane of symmetry. We tilted by moving the surface normal in the plane defined by itself and the $[\bar{1}2\bar{1}]$ surface direction. As a consequence, the threefold rotational symmetry is broken, a mirror plane remains, and we have two equivalent beams out of three.

Dynamical LEED calculations were performed using the package CLEED developed by Held.[12] Theoretical I-V curves are computed by layer-doubling[13] except where convergence is poor due to short distances between layers (e.g., the silicon bilayer). For these cases the program automatically switches to a real-space composite layer method.[14] From a suite of different R factors quantifying the agreement between the theoretical and the experimental curves we have favored Pendry's R factor on account of its robustness and the ample experience with assessing confidence on structures from the different parameters entering the theoretical search. The CLEED package includes an automated optimization procedure with several choices; we have used the Nelder and Mead downhill simplex.[15] While this method performs efficiently a true multidimensional minimization, it is only expected to work well in the vicinity of a global minimum, which is enough for our purposes. Finally, $l_{\max}=8$ was used for the phase shifts, that were obtained from MUFPOT.[13]

The atomic positions of the Y and Si atoms were varied in five surface planes: the last Si bulk bilayer, the Y layer, and the Si surface bilayer. Deeper Si atoms were held at bulk positions. As the LEED pattern stays always a $p(1\times1)$, we have used the Si lattice parameter to describe cells inside different planes ($a_p=3.84$ Å). However, for the sake of completeness, we have tried also minimizing this value, resulting in a small decrease in the best R factor (from 0.21 to 0.20) for a 5% increase in that parameter. A similar effect has been previously reported in the literature, which seems to be related to assuming a constant real part for the optical potential.[16] As we have made no attempt to optimize an energy-dependent self-energy (neither for the real nor for the imaginary part), we interpret this effect as due to the limitations of our calculations and we disregard it as unphysical. Other nonstructural parameters considered in the analysis were the isotropic atomic rms vibrational displacements for the aforementioned five layers, and the bulk value, the real and imaginary part of the inner potential, and the polar incidence angle with respect to the surface normal. Final values for all these parameters can be found in Table II.

The density-functional calculations have been performed using the VASP code.[17] The generalized gradient approximation[18] (GGA) has been used for the exchange and correlation terms. Electron-ion interaction is described by pseudopotentials. The ultrasoft pseudopotentials[19] limit the size of the plane wave basis (cutoff 200 eV). Y and Si ultrasoft pseudopotentials have been extensively checked and used in previous studies.[20,21] We especially showed that Y $4p$ semicore states have to be treated as valence states. Integration in the Brillouin zone is done on a set of 100 irreducible k points generated from the Monckhorst-Pack scheme. The supercell used to describe the surface consists of four silicon bilayers plus one yttrium layer and one silicon bilayer on one side. On the other side, dangling bonds are saturated by H atoms. The theoretical bulk silicon lattice parameter (5.463 Å) has been used. All atoms are allowed to relax.

III. RESULTS AND DISCUSSION

For a complete determination of the atomic structure, we first have to consider all the possible stacking configurations for the atomic layers, and to compare the calculated LEED I-V curves for every model with the experimental curves. As there is no previous quantitative information on this structure, we assume the starting point to be dictated by other RE silicides.[4,6,22,23] Therefore, we have considered the six most

TABLE I. Optimum Pendry R factor for some geometrical models.

Y position with respect to Si(111) interface	Si bilayer orientation	
	Rotated 0°	Rotated 180°
T_4 site	0.53	0.29
H_3 site	0.89	0.67
On top site	0.71	0.75

realistic possibilities of stacking. They are the same set of structures as Kitayama *et al.*[7] tried for their LEED I-V work on $HoSi_2$. Depending on the position of the Y atom with respect to the Si interface atoms we have considered a T_4 position, a H_3 position, and an atop position. For all of them the topmost Si double layer could be in the same orientation or rotated 180° with respect to the bulk orientation. Table I summarizes the optimum Pendry R_p factor for the different tested models. From the R_p results, five of these models can be directly ruled out due to their high R_p value. We have found that the configuration with the lowest R factor corresponds to a geometrical arrangement similar for all rare-earth silicides. This model is schematically represented in Fig. 1.

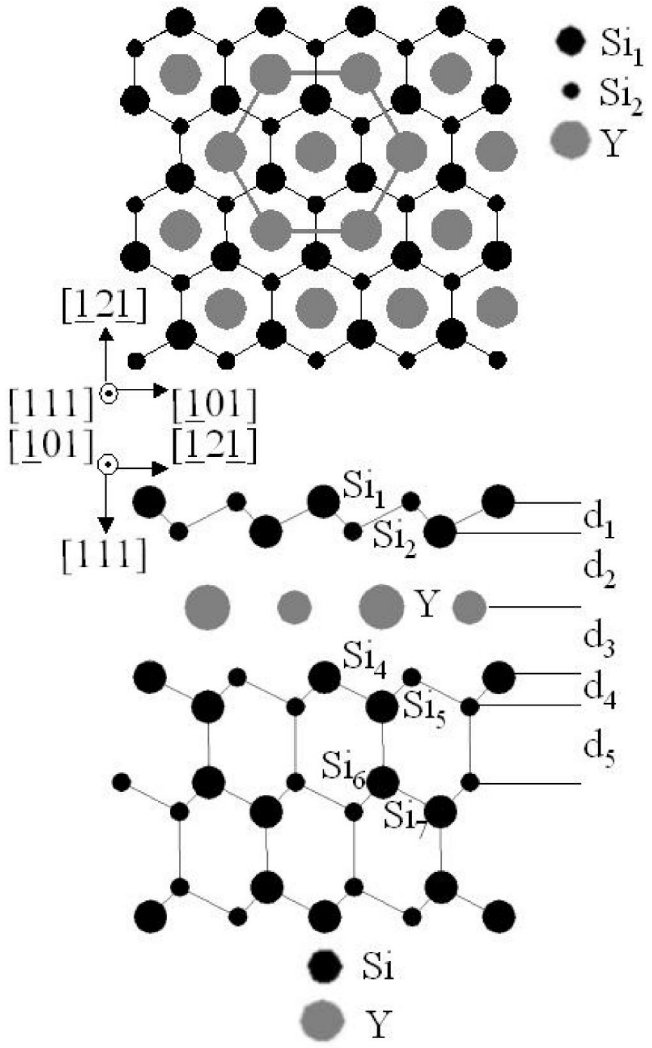

FIG. 1. Top and side views of the structural model for the $p(1\times1)$-$YSi_2/Si(111)$.

TABLE II. Nonstructural parameters by layers. There is a remarkable change in the R factor corresponding to the vibrations. On the left, rms displacements obtained for each atom from the bulk Debye temperature, and on the right column, the optimized values for each surface layer. The real and the imaginary part of the inner potential are also summarized.

$V_{\text{real part}} = -10$ eV, $V_{\text{imaginary part}} = 3.9$ eV		
	Bulklike values $\langle \Delta r \rangle$	Best-fit values $\langle \Delta r \rangle$
Si_{bulk}	0.06	0.06
Si_5	0.06	0.06
Si_4	0.06	0.06
Y	0.09	0.08
Si_2	0.06	0.13
Si_1	0.06	0.17
R_P	**0.4581**	**0.2078**

Once the geometrical arrangement was established, we focused on finding accurate values for the interatomic distances involved in the system. We have performed a careful minimization process through several stages. After a first search for the structural parameters and an estimation of the nonstructural parameters, a refinement of the R_p was carried out. In this process, we have realized that a correct guess for the thermal vibrational amplitudes at each surface layer is necessary to get the R factor to low-enough values to make it significant. This point is illustrated by reference to Table II, where R-factor values corresponding to the optimum geometry given in Table III, are compared for two cases: on the left rms displacements obtained for each atom accordingly to their bulk Debye temperature (e.g., 645 K for Si and 280 K for Y), compared to the optimized values for each surface layer given on the right column. The dramatic change in the R factor down from 0.46 to 0.21 illustrates well enough the importance of vibrations in this system. In our case, visual agreement between experimental I-V curves and theoretical curves computed with vibrations described by a bulk Debye temperature were not satisfactory enough, nor such a high value as $R_p = 0.46$ could be considered a reasonable fit. Following Spence *et al.*[8] we have also tried increasing vibrations in the two silicon upper layers by a factor of $\sqrt{2}$: The corresponding reduction in the R factor from 0.46 to 0.37, although already significant, is not completely satisfactory. Those values are close enough to the R factor obtained by Kitayama *et al.*[7] in their LEED analysis for $HoSi_2$ ($R_p = 0.42$), and one may speculate about the influence of vibrations in the analysis of this system.

The procedure used to adjust the structural parameters was performed as follows. The five planes (see Fig. 1) were varied independently. After this procedure, we obtained fairly good agreement between calculations and experiment. Then, we adjusted again the nonstructural parameters in order to minimize the R_p and, finally, we moved the last two

TABLE III. Atomic distances between layers calculated by LEED and by density-functional theory compared with the results from other authors. The distances referred to are from Fig. 1.

	$DyGe_2$	$HoSi_2$		$ErSi_2$		YSi_2	
	MEIS[a]	LEED[b]	MEIS[c]	MEIS[c]	SXRD[d]	DFT	LEED *I-V*
Si_1-Si_2(Ge_1-Ge_2) (Å)	1.08±0.02	0.82	0.88±0.03	0.92±0.03	0.82±0.03	0.789	0.79±0.04
Si_2(Ge_2)-*R* (Å)	1.71±0.02	1.88	1.80±0.03	1.77±0.03	1.78±0.08	1.769	1.85±0.04
R-Si_4(Ge_4) (Å)	2.9±0.1	2.03	2.10±0.06		2.30±0.06	2.052	2.08±0.03
Si_4-Si_5(Ge_4-Ge_5) (Å)	0.78±0.07	1.01	0.90±0.06		0.80±0.06	0.903	0.90±0.04
Si_5-Si_6(Ge_5-Ge_6) (Å)		2.30					2.32±0.08
Si_6-Si_7(Ge_6-Ge_7) (Å)	0.84			0.78			

[a]Reference 8.
[b]Reference 7.
[c]Reference 6.
[d]Surface X-ray diffraction (SXRD). Lohmeier *et al.* (Ref. 23) in this reference also reported similar results from MEIS experiments.

layers (Si_1 and Si_2 in Fig. 1) to optimize their values. The R_p variations as a function of the distance between Y and Si_2 (d_2) and the buckling between Si_1 and Si_2 (d_1), keeping the others distances fixed, is shown in the 2D map represented in Fig. 2. The lower R_p corresponds to the darker gray shade. In the figure, the statistical variance (RRP=0.03) is also represented. From this value, we estimate errors in the structural determination as shown in shadowed areas in Fig. 2.

This map shows three local minima of the *R* factor for 0.33, 0.79, and 1.6 Å with *R* factors of 0.21, 0.21, and 0.33, respectively. These values look like multiple coincidences for the last two Si layer distances. Usually, local minima are discarded by its higher *R* factor compared with the real one.

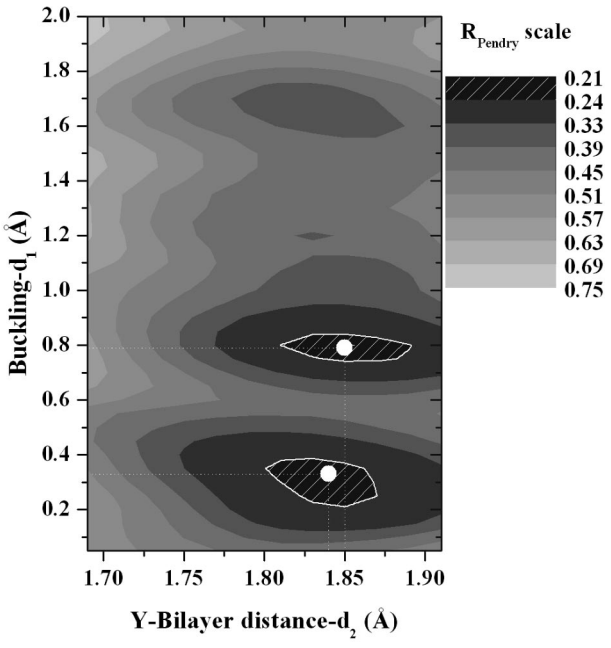

FIG. 2. Variation of the Pendry *R* factor as a function of two distances: The Y-bilayer spacing and the buckling of the top layer. The shadowed areas represent the variance of R_P around the minima, and the white points represent the minima of the *R* factor. This figure shows the multiple occurrence of local minima.

However, in this case, the values at 0.33 and 0.79 Å (white spots in Fig. 2) present the same value for the *R* factor (0.21) and are more than one variance apart in parameter space, so we cannot choose one from the LEED analysis at normal incidence alone. One possibility would be that the minima correspond to different structures coexisting on the surface. However, the calculated curves for both structures are so similar that we take it as a case for extending the structural search to new conditions that could eventually discriminate between both minima, a case that indeed has been confirmed by a following analysis based in non-normal incidence of the primary beam.

In order to distinguish between the two minima, we have taken several actions. First we have recorded and analyzed *I-V* curves out of normal incidence. Our purpose was to calculate the atomic structure for each set of curves at different angles, expecting that for some angles the spurious minima will be higher than the real minima making possible the discrimination.

Therefore, we have measured $I(E)$ spectra for several incidence angles of the electron beam with respect to the surface normal. The azimuthal angle was set in such a way that we varied the polar angle following the $[\bar{1}2\bar{1}]$ surface direction. To determine the value of polar angles with precision, we have calibrated our sample manipulator before the experiment. This can lead to typical errors of about 2°. Additionally, the polar angles have been obtained from the LEED pattern by an iterative procedure.[12] The rms deviations obtained for the incident angle are always better than 0.2°. Finally, we have adjusted the polar angle by optimizing the Pendry *R* factor between experimental and theoretical *I-V* curves: the maximum deviation between this last procedure, considered to be the best, and the previous ones has always been below 0.4°.

In Fig. 3 we have plotted R_p for different experimental incidences comparing with the corresponding theoretical calculations around the angles previously determined by direct calibration of the manipulator and nonlinear fit as explained above. Results are shown for the two best minima previously identified: dotted line corresponds to the 0.33-Å structure, while solid line corresponds to the buckling 0.79-Å structure.

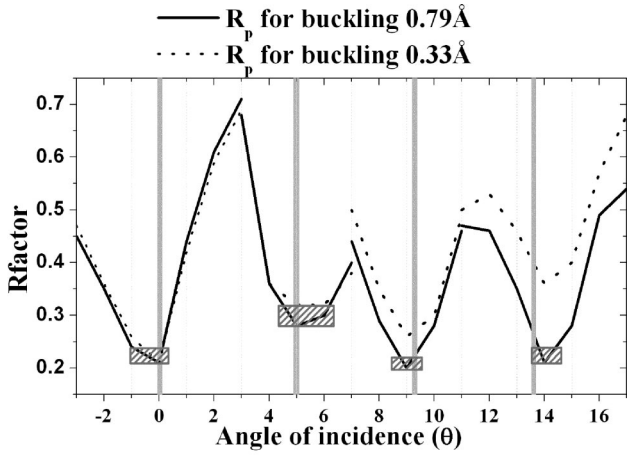

FIG. 3. Variation of the Pendry R factor as a function of the electron-beam incidence angle for the structure with a buckling of 0.33 Å (dotted line) and 0.79 Å (solid line). The striped areas represent the variance of the R_P around the minima, and the vertical lines represent the angles with their errors calculated by the program referred in Ref. 11.

The best-fit values correspond to $\theta=4°$, 9°, and 14°. The statistical variance for R_p, RRP, and the results obtained from the referred program are also plotted (shaded region) for each angle. As commented above, values for the angle determined from all the methods are consistent.

Figure 3 shows that around $\theta=0°$ curves for both structures are fairly close and therefore cannot be distinguished from this analysis. However, when the angle is increased, the differences become more apparent. At $\theta=4°$ differences

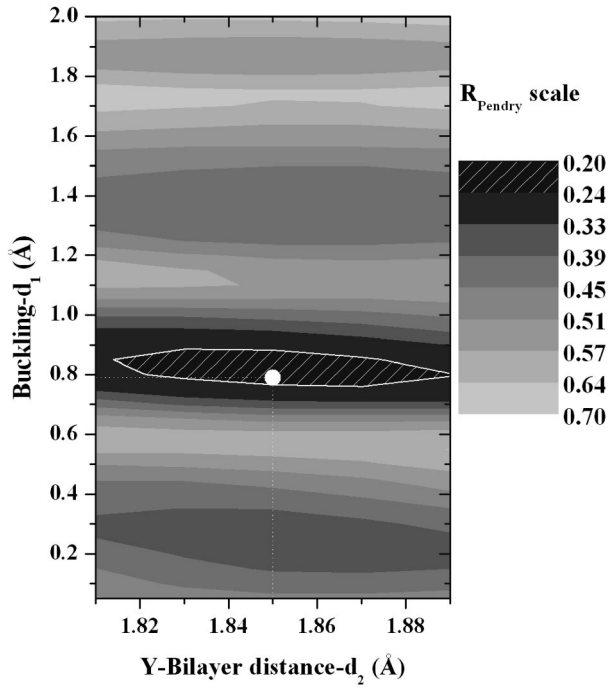

FIG. 4. Variation of the Pendry R factor as a function of the Y-bilayer spacing and the buckling of the top layer, for a set of experimental curves recorded 14° out of normal incidence.

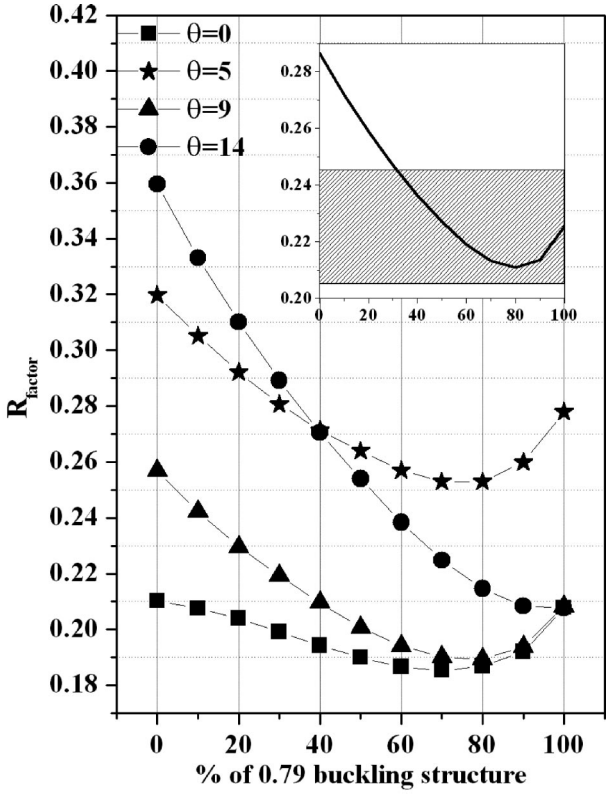

FIG. 5. R-factor evolution obtained by comparing the experimental curves for every incidence angle with a linear combination of the calculated I-V curves for the two local minima. The inset represent an average of all of them. The shadowed part represents the statistical variance of the R factor.

start to show, but still are within the experimental error and it is not possible to discriminate. For $\theta=9°$ and $\theta=14°$, however, we clearly observe that 0.79 Å represents a lower minimum than 0.33 Å. The relatively high value found for R_p in the case of $\theta=4°$ can be explained from the lack of data for the (2,0) beam, that in this case is inside the gun region. Accordingly, the variance for R_p in this case is higher than that in the others. To further illustrate this discussion we present the Pendry R factor map for $\theta=14°$ (Fig. 4). Comparing Figs. 2 and 4, it is possible to see the difference in the values of both minima: at 0.33 Å R_p is 0.36, while at 0.79 Å, 0.21. Then, even with the statistical variance (RRP=0.03) the minimum at 0.33 Å is far from the other, and it is clear that the minimum for 0.79 Å represents the best fit to the structure.

An interesting point is to discern whether or not both minima correspond to different ''real'' domains that could coexist on the surface under the current preparation conditions. If this were the case, and assuming that both domains are big enough so they add incoherently, a linear combination of the calculated I-V curves should lead to lower R factor values. This is illustrated in Fig. 5, where we have represented the R factor found by comparing the experimental curves with a calculated one, obtained by mixing both structures in a percentage. It is shown for the different studied incidence angles. It can be seen that the combination presents a shallow minimum for all incidence (i.e., inside the

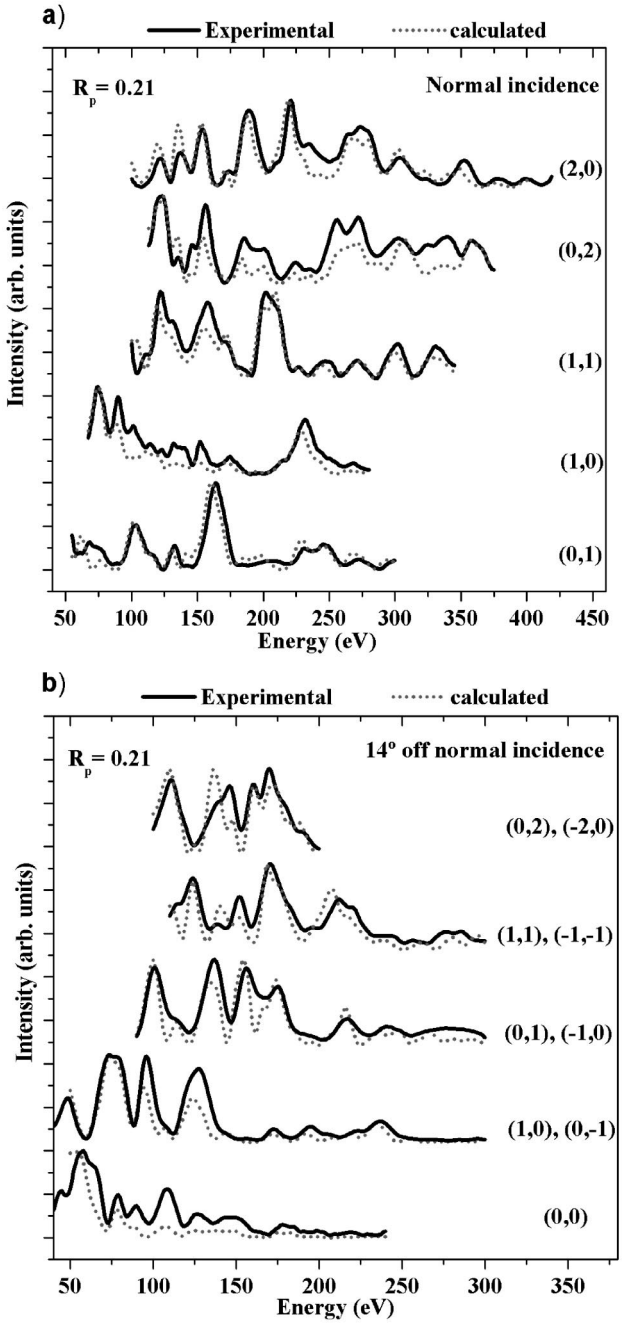

FIG. 6. Best-fit experimental and calculated $I(E)$ curves for the YSi_2 (a) normal incidence and (b) angle of incidence 14° out of normal incidence.

R factor variance), except for the one at 14°. An average of all of them is shown in the inset. The statistical variance is indicated in the figure by a shadowed area. It is clear from the figure that the minimum appearing at around 80% of the structure at 0.79 Å is not significant enough and can be discarded from the behavior at large angles, in particular 14°. This minimum is within the variance, and therefore we can conclude that in our case both curves correspond to multiple coincidences on the *R*-factor minimum rather to the coexistence of several surface structures.

Furthermore, for both structures we have analyzed the R_p for each beam separately, and the values of *R* factors different from Pendry's. All these procedures favor 0.79Å as the real distance.

Figure 6 shows the best fit for the experimental curves obtained for normal incidence (upper figure) and 14° off normal incidence towards the [121] surface direction (lower figure). The best *R* factor is 0.21 for both cases and the visual agreement is very good. The structural parameters of the best fit structure are summarized in Table III.

We have also studied this system independently by performing DFT calculations where total energies for different structures are obtained. Our goal is to find the more stable geometry and to compare it with the experimentally determined LEED distances. The results are summarized in Table III. The good agreement between theory and experiment is noteworthy. Differences between them are within the experimental error bar. We notice that the 0.33 Å structure it 0.191 eV/cell higher in energy than the 0.79-Å structure. Thus, the DFT analysis also points to the same structure as the LEED experiment.

As can be seen from Fig. 1, the surface Si plane relaxes. The Si bilayer width equals 0.79 Å both from theory and experiments, which is also compatible with other reported rare-earth silicide relaxed distances in the surface. This effect was also found at the $YSi_{1.7}$ surface, with 0.76 Å,[20] or in $ErSi_{1.7}$, with 0.8 Å.[24] These relaxations have been related to a way of releasing the stress within the silicon plane, and compared to the bulk silicide geometry, which can be thought of as a buckling of the surface layers. The other distances (d_2, d_3) are also close to the 3D silicide surface interlayer distances, which are around 1.9 and 2.07 Å respectively.

The electron from the Si surface broken bond backbonds and hybridizes with the underlying Y atom forming a $Si3s3p/Y5d6s6p$ orbital. The electronic structure for this system has been described by Staufer *et al.* in Ref. 5. In this work we proved that d_{12} is almost equal to the Si bulk, indicating that the in-plane bonding of the Si atoms is strong and localized and is not affected by the backbond with the Y atoms underneath. However, the vertical relaxation d_2 distance is 11% contracted with respect to d_3.

In Table III is clear that all the 2D silicides studied until now present interatomic distances very close to each other. These similarities are not surprising for Ho and Er, which are adjacent in the periodic table and only differ in one $4f$ electron. However, Y has no $4f$ electrons and these coincidences indicate that they do not participate in the electronic bonding. Er, Ho, and Y present the same trivalent character, and the differences between them come from the occupation of the inner $4f$ orbitals; therefore it is not surprising that they form silicides with the same lattice parameters, as evidenced in Table III.

From this structural determination it is worth noticing the enhancement of the distance between the last two Si layers (d_4), which has increased by 0.12 Å with respect to the Si(111) plane. This effect has also been reported for $HoSi_2$. The rare-earth atom, in a T_4 position, maximizes the number of bonds with the Si layers. The fact that the Si_4 atoms are outward displaced by 0.12 Å could be understood as a way

for the Y atom to decrease the bond length with these atoms, and a tendency to make the bond distance uniform with the surrounding Si atoms. Briefly the Si_4-Y bond length is reduced from 3.12 Å (for an unchanged Si bulk distance of 0.78 Å) to 3.04 Å, a value which is closer to the Si_2-Y (2.88 Å) and to the Si_5-Y (2.98 Å) bond lengths.

IV. CONCLUSIONS

By means of a detailed LEED analysis and DFT calculations, we have determined the atomic structure of $p(1\times1)$ YSi_2 epitaxially grown on Si(111). The geometric atomic structure of this silicide is similar to other 2D rare-earth silicides. The surface termination consists of a relaxed Si bilayer, with the Y atoms located in a T_4 site with respect to the Si(111) interface. This conclusion has been obtained by a detailed analysis of non-normal incidence LEED *I-V* curves.

ACKNOWLEDGMENTS

We acknowledge helpful advice with CLEED from G. Held. This work has been financially supported through Grant Nos. PB98-0524 and FEDER 1FD97-1358, one of the authors (L.M.) wishes to thank J. Hafner and G. Kresse for the VASP code.

*Current address: I. Physikalisches Institut RWTH-Aachen, 52056 Aachen, Germany.

[1] R. D. Thompson, B. Y. Tsaur, and K. N. Tu, Appl. Phys. Lett. **38**, 535 (1981).
[2] K. N. Tu, R. D. Thompson, and B. Y. Tsaur, Appl. Phys. Lett. **38**, 626 (1981).
[3] P. Paki, U. Kafader, P. Wetzel, C. Pirri, J. C. Peruchetti, D. Boltont, and G. Gewinner, Phys. Rev. B **45**, 8490 (1992).
[4] P. Wetzel, C. Pirri, P. Paki, D. Bolmont, and G. Gewinner, Phys. Rev. B **47**, 3677 (1993); P. Wetzel, C. Pirri, D. Bolmont, and G. Gewinner, Appl. Surf. Sci. **65**, 718 (1993).
[5] L. Stauffer, A. Mharchi, C. Pirri, P. Wetzel, D. Boltont, and G. Gewinner, Phys. Rev. B **47**, 10 555 (1993).
[6] D. J. Spence, S. P. Tear, T. C. Q. Noakes, and P. Bailey, Phys. Rev. B **61**, 5707 (2000).
[7] H. Kitayama, S. P. Tear, D. J. Spence, and T. Urano, Surf. Sci. **482**, 1481 (2001).
[8] D. J. Spence, T. C. Q. Noakes, P. Bailey, and S. P. Tear, Phys. Rev. B **62**, 5016 (2000).
[9] C. Polop, C. Rogero, J. L. Sacedón, and J. A. Martín Gago, Surf. Sci. **482**, 1337 (2001).
[10] J. B. Pendry, J. Phys. C **13**, 937 (1980).
[11] M. A. Van Hove, W. H. Weinberg, and C. M. Chan, *Low Energy Electron Diffraction* (Springer, Berlin, 1986). Program for the determination of the angle of incidence is in Appendix B.
[12] G. Held, Department of Chemistry, University of Cambridge, U.K.
[13] J. B. Pendry, *Low-Energy-Electron Diffraction* (Academic, London, 1974).
[14] M. A. Van Hove and S. Y. Tong, *Surface Crystallography by LEED* (Springer, Berlin, 1979).
[15] W. H. Press, S. A. Teukolsky, W. T. Vetterling, and B. P. Flannery, *Numerical Recipes* (Cambridge University Press, Cambridge, 1992).
[16] S. Walter, V. Blum, I. Hammer, S. Muller, K. Heinz, and M. Giesen, Surf. Sci. **458**, 155 (2000).
[17] G. Kresse and J. Hafner, Phys. Rev. B **47**, 558 (1993); G. Kresse, Ph.D. thesis, Technische Universität Wien, (1993).
[18] J. P. Perdew and Y. Wang, Phys. Rev. B **33**, 8800 (1986).
[19] D. Vanderbilt, Phys. Rev. B **41**, 7892 (1990); G. Kresse and J. Hafner, J. Phys.: Condens. Matter **6**, 8245 (1994).
[20] L. Magaud, A. Pasturel, G. Kresse, and J. Hafner, Phys. Rev. B **55**, 13 479 (1997).
[21] L. Magaud, A. Pasturel, G. Kresse, and J. Hafner, Phys. Rev. B **58**, 10 857 (1998).
[22] M. H. Tuilier, P. Wetzel, C. Pirri, D. Bolmont, and G. Gewinner, Phys. Rev. B **50**, 2333 (1994); H. Tuilier, C. Pirri, P. Wetzel, and G. Gewinner, Surf. Sci. **307**, 710 (1994).
[23] M. Lohmeier, W. J. Huisman, G. ter Horst, P. M. Zagwijn, E. Vlieg, C. L. Nicklin, and T. S. Turner, Phys. Rev. B **54**, 2004 (1996).
[24] L. Stauffer, A. Mharchi, S. Saintenoy, C. Pirri, P. Wetzel, D. Bolmont, and G. Gewinner, Phys. Rev. B **52**, 11 932 (1995).